

## More detailed study of fission dynamics in fusion-fission reactions within a stochastic approach

P. N. Nadtochy, G. D. Adeev, and A. V. Karpov

*Department of Theoretical Physics, Omsk State University, Mira prospect 55-A, Omsk 644077, Russia*

(Received 31 July 2001; revised manuscript received 21 March 2002; published 11 June 2002)

A stochastic approach based on three-dimensional Langevin equations was applied to a more detailed study of fission dynamics in fusion-fission reactions. The dynamical model has been developed and extended to investigate fission characteristics of light fissioning nuclei at low excitation energies. The energy dependences of an anisotropy of the fission fragment angular distribution, an evaporation residue cross section, a fission cross section, mean precission neutron, and giant dipole  $\gamma$  multiplicities have been analyzed for the  $^{16}\text{O} + ^{208}\text{Pb}$ -induced fission of  $^{224}\text{Th}$ . Also, dependence of the precission neutron multiplicity on the fragment mass asymmetry and total kinetic energy have been calculated. Analysis of the results shows that not only characteristics of the mass-energy distribution of fission fragments, but also the mass and kinetic-energy dependence of the precission neutron multiplicity, the angular anisotropy, and fission probability can be reproduced using a modified one-body mechanism for nuclear dissipation with a reduction coefficient of the contribution from a wall formula  $k_s = 0.25 - 0.5$  for compound nuclei  $^{172}\text{Yb}$ ,  $^{205}\text{Fr}$ ,  $^{215}\text{Fr}$ , and  $^{224}\text{Th}$ . Decrease of the precission neutron multiplicities with fragment mass asymmetry is due to a decrease of the fission time. The results obtained show that precission neutrons are evaporated predominantly from the nearly spherical compound nucleus at an early stage of fission process before the saddle point is reached. From performed analysis one can conclude that coordinate-independent reduction coefficient  $k_s$  is not compatible with simultaneous description of the main fission characteristics for heavy fissioning systems  $^{256}\text{Fm}$  and  $^{252}\text{Fm}$ .

DOI: 10.1103/PhysRevC.65.064615

PACS number(s): 25.85.-w, 21.10.Gv, 05.10.Gg

### I. INTRODUCTION

The most detailed and systematic information on large-scale collective nuclear motion presently available from heavy-ion reactions has been accumulated from measuring the multiplicities of evaporated particles, especially neutrons, in fusion-fission reactions in coincidence with mass and kinetic-energy distributions of fission fragments [1–3]. Analysis of these data and further references are presented in review [4]. Three-dimensional Langevin calculations of the fission fragment mass-energy distributions (MED) have been carried out quite recently [5,6]. In the dynamical model [5,6] the evolution of three most important shape parameters: elongation, constriction, and mass asymmetry is described by the coupled Langevin equations. Along each stochastic Langevin trajectory an evaporation of light particles is considered. The results of these calculations show that the three-dimensional Langevin dynamics makes it possible to describe comprehensively characteristics of the MED of fission fragments and the mean precission neutron multiplicity. The above-mentioned results can be considered as promising and encouraging for further development and extension of the stochastic approach to fission dynamics based on the three-dimensional Langevin equations.

The mass and kinetic-energy dependence of the precission neutron multiplicities have been studied in the experiments [1–4] in addition to the parameters of the fission fragment MED and the mean precission neutron multiplicity. On the other hand, descriptions and explanations of such exclusive data as the mass and kinetic-energy dependence of the precission neutron multiplicities have not been undertaken in full extent so far. It is a crucial test for theoretical models including the stochastic approach based on the Langevin equations. So the available experimental data of

the precission neutron multiplicities as a function of the fragment mass asymmetry and kinetic energy have to be compared more closely with theoretical findings by means of the three-dimensional Langevin dynamical calculations. In the present paper we extend the investigations recently carried out in Refs. [5,6] to calculate the mass and kinetic-energy dependence of the precission neutron multiplicities, the dependences of the mean precission neutron multiplicity  $\langle n_{\text{pre}} \rangle$ , fission probability  $P_f$ , and some other observables on excitation energy.

The aim of our study is twofold. First, we would like to analyze and elucidate correlations between the precission neutron multiplicities and the fission fragment MED. The second one concerns an investigation of the mean precission neutron multiplicities  $\langle n_{\text{pre}} \rangle$ , the fission probability  $P_f$  (or survival probability), and the fission fragment angular anisotropy in a broad range of the excitation energy. Particular attention is paid to estimating the ground-state-saddle  $\langle n_{\text{pre}}^{\text{g.s.}} \rangle$  and saddle-scission  $\langle n_{\text{pre}}^{\text{ss}} \rangle$  contributions to the precission neutron multiplicity  $\langle n_{\text{pre}} \rangle$ . We investigate the influence of the ratio  $\langle n_{\text{pre}}^{\text{g.s.}} \rangle / \langle n_{\text{pre}} \rangle$  on the mass and kinetic-energy dependence of the precission neutron multiplicities and on the fission fragment angular anisotropy.

For the analysis of the mass and kinetic-energy dependence of the precission neutron multiplicities we have chosen five representative systems in the range of the masses  $A_{\text{CN}} = 172 - 256$  and the excitation energies  $E^* = 70 - 140$  MeV, which were formed in the following fusion-fission reactions:  $^{18}\text{O} + ^{154}\text{Sm} \rightarrow ^{172}\text{Yb}$  ( $E_{\text{lab}} = 159$  MeV) [1];  $^{36}\text{Ar} + ^{169}\text{Tm} \rightarrow ^{205}\text{Fr}$  ( $E_{\text{lab}} = 205$  MeV) [2];  $^{18}\text{O} + ^{197}\text{Au} \rightarrow ^{215}\text{Fr}$  ( $E_{\text{lab}} = 159$  MeV) [1];  $^{20}\text{Ne} + ^{232}\text{Th} \rightarrow ^{252}\text{Fm}$  ( $E_{\text{lab}} = 215$  MeV) [7];  $^{18}\text{O} + ^{238}\text{U} \rightarrow ^{256}\text{Fm}$  ( $E_{\text{lab}} = 159$  MeV) [1]. Theoretical calculations for

these systems within two-dimensional dynamical models also have been carried out in Refs. [8,9]. We have concentrated on the particular example of the  $^{16}\text{O}+^{208}\text{Pb}$ -induced fission of  $^{224}\text{Th}$  for the analysis of the mean precession neutron multiplicity  $\langle n_{\text{pre}} \rangle$ , the fission probability  $P_f$ , and the fission fragment angular anisotropy, because this system has been investigated carefully in both experimental [10–18] and theoretical [5,19–23] studies. It should be mentioned that similar investigations of influence of the nuclear dissipation on heavy-ion-induced fission of  $^{224}\text{Th}$  formed in the same reaction have been performed earlier by Fröbrich and co-workers [20,22,23]. They have shown that precession  $\gamma$  multiplicities and the evaporation residue cross sections are more sensitive probes for nuclear friction in fission than precession neutron multiplicities. Also, they have claimed [20] that fission fragment angular anisotropy can be affected by evaporation of presaddle neutrons and strongly depends on nuclear dissipation, in particular for compact configurations. Therefore, it is interesting to compare the results of three-dimensional Langevin calculations with those obtained by Fröbrich and co-workers and to show influence of the additional necessary collective coordinates as incorporated in the dynamical model.

In order to make the paper self-contained we shall describe in Sec. II the multidimensional Langevin equations with some technical aspects and details of the model used in the present study. Section III is devoted to the results obtained in this study and to their discussion in comparison with available experimental data. Finally, the concluding remarks are given in Sec. IV.

## II. MULTIDIMENSIONAL LANGEVIN EQUATIONS

The dynamical model has been described in detail in our previous paper [5]. Here we explain only some technical aspects of the model that have not been clarified in Ref. [5] and describe further developments. It should be stressed that no special ad hoc parameters or assumptions were introduced in the present paper. All input parameters of our dynamical model were presented in Ref. [5] and their values were determined from optimal description of the experimental MED of fission fragments and the mean precession neutron multiplicities.

In our dynamical calculations we used a slightly modified form of the  $\{c, h, \alpha\}$  parametrization [24]. In Ref. [5] we introduced a different mass asymmetry parameter scaled with elongation  $\alpha' = \alpha c^3$ . The geometrical shape parameters were chosen as collective coordinates:  $\mathbf{q} = (c, h, \alpha')$ . Multi-dimensional Langevin equations describing fission dynamics of highly excited nuclei discretized in a form convenient for numerical simulation will be given [23] as

$$p_i^{(n+1)} = p_i^{(n)} - \left( \frac{1}{2} p_j^{(n)} p_k^{(n)} \left( \frac{\partial \mu_{jk}(\mathbf{q})}{\partial q_i} \right)^{(n)} - K_i^{(n)}(\mathbf{q}) - \gamma_{ij}^{(n)}(\mathbf{q}) \mu_{jk}^{(n)}(\mathbf{q}) p_k^{(n)} \right) \tau + \theta_{ij}^{(n)} \xi_j^{(n)} \sqrt{\tau}, \quad (1)$$

$$q_i^{(n+1)} = q_i^{(n)} + \frac{1}{2} \mu_{ij}^{(n)}(\mathbf{q}) (p_j^{(n)} + p_j^{(n+1)}) \tau,$$

where  $\mathbf{q} = (c, h, \alpha')$  are the collective coordinates,  $\mathbf{p} = (p_c, p_h, p_{\alpha'})$  are the conjugate momenta,  $K_i(\mathbf{q})$  is a conservative driving force,  $m_{ij}$  ( $\|\mu_{ij}\| = \|m_{ij}\|^{-1}$ ) is the tensor of inertia,  $\gamma_{ij}$  is the friction tensor,  $\theta_{ij} \xi_j$  is a random force,  $\tau$  is the integration time step, and  $\xi_j$  is a random variable satisfying the relations

$$\langle \xi_i^{(n)} \rangle = 0,$$

$$\langle \xi_i^{(n_1)} \xi_j^{(n_2)} \rangle = 2 \delta_{ij} \delta_{n_1 n_2}. \quad (2)$$

The upper index  $n$  in Eqs. (1) and (2) denotes that related quantity is calculated at time  $t_n = n\tau$ . In these equations, and further in this paper, we use the convention that repeated indices are to be summed over from 1 to 3, and the angular brackets denote averaging over an ensemble. The strengths of the random force are related to the diffusion tensor  $D_{ij}$  by the equation  $D_{ij} = \theta_{ik} \theta_{kj}$ , which, in turn, satisfies the Einstein relation  $D_{ij} = T \gamma_{ij}$ . Here  $T$  is the temperature of the “heat bath” constituted by internal degrees of freedom. The temperature of the “heat bath” is connected with internal excitation energy  $E_{\text{int}}$  of the nucleus through the level-density parameter  $a(\mathbf{q})$  by the relation of the Fermi-gas model  $T = [E_{\text{int}}/a(\mathbf{q})]^{1/2}$ . The internal excitation energy is determined by using the energy conservation law

$$E^* = E_{\text{int}} + E_{\text{coll}}(\mathbf{q}, \mathbf{p}) + V(\mathbf{q}) + E_{\text{evap}}(t), \quad (3)$$

where  $E^*$  is the total excitation energy of the nucleus,  $E_{\text{coll}}(\mathbf{q}, \mathbf{p}) = \frac{1}{2} \mu_{ij}(\mathbf{q}) p_i p_j$  is the kinetic energy of the collective degrees of freedom,  $V(\mathbf{q})$  is the potential energy, and  $E_{\text{evap}}(t)$  is the energy carried away by evaporated particles by the time  $t$ . The coordinate-dependent level-density parameter can be expressed in the form [25]

$$a(\mathbf{q}) = a_v A + a_s A^{2/3} B_s(\mathbf{q}), \quad (4)$$

where  $A$  is the mass number of the compound nucleus, and  $B_s$  is the dimensionless functional of the surface energy in the liquid-drop model (LDM) with a sharp surface [24,26]. The values of the parameters  $a_v = 0.073 \text{ MeV}^{-1}$ ,  $a_s = 0.095 \text{ MeV}^{-1}$  in Eq. (4) have been taken from the work of Ignatyuk *et al.* [27]. It follows from the analysis [28] of existing sets of the level-density parameters that the parameters of Ignatyuk’s *et al.* lead to almost the weakest coordinate dependence of the level-density parameter. The level-density parameter  $a(\mathbf{q})$  is the most important quantity not only in the statistical model calculation of the light precession particles evaporation, but also in the dynamical calculations. It is well known [29] that for the description of an excited nuclear system the potential energy must be replaced by the free energy  $F(\mathbf{q}, T)$  in the dynamical equations. The free energy is related to the level-density parameter by the formula of the Fermi-gas model

$$F(\mathbf{q}, T) = V(\mathbf{q}) - a(\mathbf{q}) T^2. \quad (5)$$

Microscopic extended Thomas-Fermi calculations have shown [30] that Eq. (5) can be expected to be a reasonable approximation for  $T \leq 4$  MeV. A conservative driving force in Langevin equations is given by the derivative of the free energy with respect to the collective coordinates at the constant temperature:  $K_i(\mathbf{q}) = -(\partial F(\mathbf{q})/\partial q_i)_T$ . It is a noticeable extension of the model presented in Ref. [5]. It is easy to see that the driving force consists of the usual conservative force  $-(\partial V(\mathbf{q})/\partial q_i)_T$  plus a term that comes from the thermodynamic properties of the excited fissioning nucleus, which enters via the level-density parameter  $a(\mathbf{q})$ . The additional force introduced into dynamical equations by using free energy instead of potential energy effectively corresponds to the temperature-dependent term in surface energy. This kind of generalization of the surface energy calculated in Yukawa-plus-exponential model [31] has been used successfully for the simultaneous description of the fission characteristics in Refs. [32–34]. Evidently, using the free energy is more preferable than the generalization of the surface energy, including the temperature-dependent term, from the point of view of the consistency of the model.

We started modeling fission dynamics from an equilibrated spherical compound nucleus, i.e.,  $\mathbf{q}_0 = (c_0 = 1.0, h_0 = 0.0, \alpha_0' = 0.0)$ . It was supposed that the scission occurred when the neck radius of the fissioning nucleus was equal to  $0.3R_0$  [24,35] ( $R_0$  is the radius of the initial spherical nucleus). This scission condition determined the scission surface in the space of the collective coordinates. Evaporation of prescission light particles ( $j = n, p, d, t, {}^3\text{He}, \alpha, \gamma$ ) along Langevin fission trajectories was taken into account using a Monte Carlo simulation technique [23,36]. All dimensional factors were recalculated when a light prescission particle was evaporated, only dimensionless functionals of the rotational, Coulomb, and nuclear energies were not recalculated. This procedure provides a good accuracy in calculating the potential energy. If several different particles have been evaporated, the difference between the exact value of the potential energy and the value found without recalculation of the dimensionless functionals does not exceed 1 MeV. The loss of angular momentum was taken into account by assuming that light particles carry away  $l_j = 1, 1, 2, 1, 1, 2, 1$  ( $\hbar$ ) [23].

In contrast to Ref. [5] we have studied a few compound nuclei with a rather low fissility. This has been only possible by switching over to a statistical model description with a Kramers-type fission decay width after delay time, when stationary flux over the saddle point is reached. This procedure has been first proposed in Ref. [36]. An appropriate expression for the fission width that is the generalization of Kramers formula to the multidimensional case [37,38] reads

$$\Gamma_f = \omega_K \left( \frac{\det \Omega_{ij}^2(\mathbf{q}_{\text{g.s.}})}{\det |\Omega_{ij}^2(\mathbf{q}_{\text{sd}})|} \right)^{1/2} \exp\{-[F(\mathbf{q}_{\text{sd}}) - F(\mathbf{q}_{\text{g.s.}})]/T\}, \quad (6)$$

where the frequency tensors at ground state and saddle point,

$$\Omega_{ij}^2(\mathbf{q}_{\text{g.s.}}) = \mu_{ik}(\mathbf{q}_{\text{g.s.}}) \left( \frac{\partial^2 F(\mathbf{q})}{\partial q_k \partial q_j} \right)_{\mathbf{q}=\mathbf{q}_{\text{g.s.}}},$$

$$\Omega_{ij}^2(\mathbf{q}_{\text{sd}}) = \mu_{ik}(\mathbf{q}_{\text{sd}}) \left( \frac{\partial^2 F(\mathbf{q})}{\partial q_k \partial q_j} \right)_{\mathbf{q}=\mathbf{q}_{\text{sd}}},$$

are determined by the inverse mass and by the curvature tensors. The Kramers frequency  $\omega_K$  is determined from the algebraic equation

$$\det[E(2\pi\omega_K/\hbar)^2 + (2\pi\omega_K/\hbar)\mu_{ik}(\mathbf{q}_{\text{sd}})\gamma_{kj}(\mathbf{q}_{\text{sd}}) + \Omega_{ij}^2(\mathbf{q}_{\text{sd}})] = 0, \quad (7)$$

where  $E$  is the unit matrix, the coordinates  $\mathbf{q}_{\text{sd}}$  and  $\mathbf{q}_{\text{g.s.}}$  determine the saddle point and the ground state, respectively. The fission probability  $P_f$  is calculated as  $P_f = N_f/(N_f + N_{\text{ER}})$ , where  $N_f$  is the number of fission events and  $N_{\text{ER}}$  is the number of evaporation residue events. A dynamical trajectory will either reach the scission surface, in which case it is counted as a fission event; or if the excitation energy for a trajectory that is still inside the saddle reaches the value  $E_{\text{int}} + E_{\text{coll}}(\mathbf{q}, \mathbf{p}) < \min(B_j, B_f)$  the event is counted as evaporation residue ( $B_j$  is the binding energy of the particle  $j$ ).

### III. RESULTS AND DISCUSSIONS

#### A. Mass and kinetic-energy dependence of the prescission neutron multiplicities

We present further calculated results for two values of the reduction coefficient of the contribution from the wall formula:  $k_s = 0.25$  and  $k_s = 0.5$ . These values of  $k_s$  do not contradict the value of  $k_s = 0.27$ , which was obtained [39] independently of fission from analyzing experimental data on the widths of giant resonances. The values of  $k_s = 0.25$  and  $k_s = 0.5$  do not contradict the limits  $0.2 < k_s < 0.5$ , which were obtained [40] from comparison of the calculated results with the experimental data of the mean total kinetic energy of fission fragments  $\langle E_K \rangle$  for fissioning nuclei throughout the periodic system. Our previous results [5] also show that the calculated parameters of the fission fragment MED and the mean prescission neutron multiplicities are found to be in a good quantitative agreement with the experimental data for the compound nucleus  ${}^{215}\text{Fr}$ ,  ${}^{205}\text{Fr}$  at the values of  $0.25 < k_s < 0.5$  and for the compound nucleus  ${}^{252}\text{Fm}$ ,  ${}^{256}\text{Fm}$  at the values of  $k_s \approx 0.25$ .

Very detailed and systematized data [1] show a parabolic mass dependence of the prescission neutron multiplicities  $\langle n_{\text{pre}}(M) \rangle$  with a maximum value  $\langle n_s \rangle$  for symmetric fission and a decrease for asymmetric one as displayed in Fig. 1(a). The dependence of  $\langle n_{\text{pre}}(M) \rangle$  can be parametrized by [4]

$$\langle n_{\text{pre}}(M) \rangle = \langle n_s \rangle - c_{\text{pre}}(M_s - M)^2, \quad (8)$$

where  $M_s$  is the fission fragment mass for the symmetric mass division.

The calculated dependences  $\langle n_{\text{pre}}(M) \rangle$  were approximated by a parabolic polynomial expression given by Eq. (8) using the least-squares method. The calculated values of  $c_{\text{pre}}$  are presented in Table I. Decrease of the prescission neutron multiplicities with the fragment mass asymmetry is due to a decrease of the fission time  $t_f$ . The mean fission time  $\langle t_f \rangle$  for

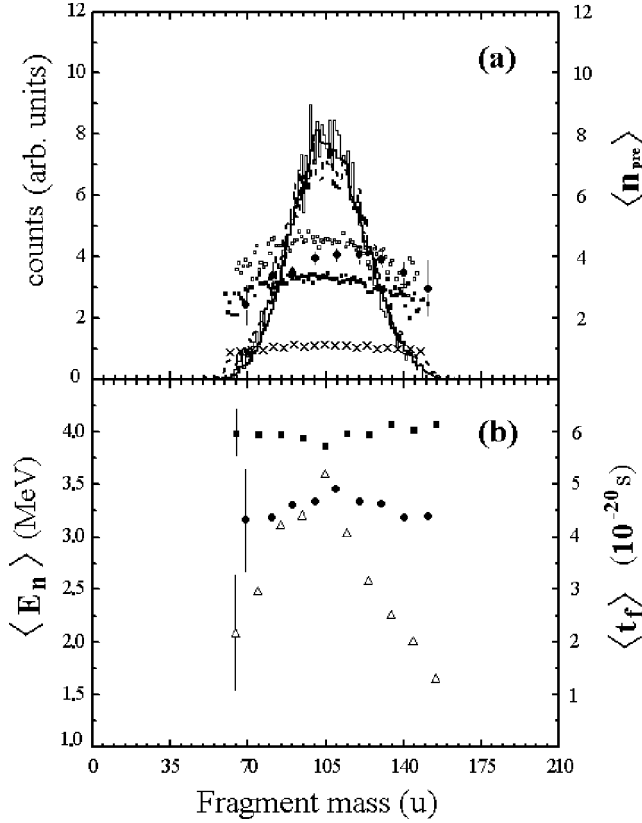


FIG. 1. (a) The mass distribution (thick solid histogram) measured in coincidence with the precission neutron multiplicities  $\langle n_{pre}(M) \rangle$  (filled circles) is compared with the theoretical calculations for the compound nucleus  $^{215}\text{Fr}$ . The experimental data have been taken from Ref. [1]. The thin solid histogram and filled squares correspond to the mass distribution and the precission neutron multiplicities calculated with  $k_s = 0.25$ , whereas the dashed histogram and open squares correspond to the results with  $k_s = 0.5$ . The crosses are the mass dependence of the precission neutron multiplicities  $\langle n_{pre}(M) \rangle$  obtained in calculations where  $\langle n_{pre}^{g.s.} \rangle = 0$  (see text). (b) The filled circles and filled squares are the experimental and theoretical (calculated with  $k_s = 0.25$ ) mass dependence of the precission neutron kinetic energies. The open triangles is the theoretical mass dependence of the fission time  $\langle t_f(M) \rangle$  calculated with  $k_s = 0.5$ , whereas filled triangles correspond to the results obtained in calculations where  $\langle n_{pre}^{g.s.} \rangle = 0$ .

the symmetric mass division is nearly two times larger than that for the asymmetric one [see Fig. 1(b)] for the compound nucleus  $^{215}\text{Fr}$ . We present in Table I the ratio  $\langle t_f^{asym} \rangle / \langle t_f^{sym} \rangle$  where  $\langle t_f^{sym} \rangle$  is the mean fission time for symmetric mass division and  $\langle t_f^{asym} \rangle$  is the mean fission time for mass ratio  $A_1/A_2 = 0.7$  ( $A_1$  and  $A_2$  are the mass numbers of the light and heavy fragments, respectively). For the explanation of the observed dependences  $\langle n_{pre}(M) \rangle$  and  $\langle t_f(M) \rangle$  it is useful to show where the precission neutrons are evaporated. Figure 2 shows the percentage yield of the precission neutron multiplicities ( $Y_n$ ) as a function of the elongation parameter  $c$  for the compound nuclei  $^{215}\text{Fr}$  and  $^{252}\text{Fm}$ . Our calculations show that an appreciable part of the precission neutrons is evaporated from the nearly spherical compound nucleus at an early stage of fission process before the saddle point is

reached. The same result was obtained earlier in Ref. [28], where the ratio  $\langle n_{pre}^{g.s.} \rangle / \langle n_{pre} \rangle$  was equal to 0.5 for the reaction  $^{16}\text{O} + ^{197}\text{Au} \rightarrow ^{213}\text{Fr}$  ( $E^* = 120$  MeV). The disagreement between the results of our calculations and those obtained in Ref. [28] is due to the number of the considered collective coordinates and different deformation dependence of the nuclear friction. We describe fission process using three collective coordinates, whereas only one collective coordinate (elongation parameter) was involved in Ref. [28]. Fissioning compound nuclei will stay for much longer time near the ground state region in three-dimensional Langevin calculations than in one-dimensional ones, because in the ground state region the potential energy weakly depends on the collective coordinates  $h, \alpha'$ . The kinetic energies of the evaporated precission neutrons ( $\langle E_n \rangle$ ) will not depend on the fragment mass asymmetry [see Fig. 1(b)], because an appreciable part of the precission neutrons is evaporated nearby the ground state region, where all fissioning nuclei have approximately equal temperature at an early stage of fission process. Different Langevin trajectories will reach the relevant conditional saddle point at different times due to a random nature of decay. If a fissioning system reaches the relevant conditional saddle point quickly and emits only few neutrons, then it will keep a greater part of the excitation energy. Such fissioning system will have a good chance of reaching the scission surface quickly and having a large final mass asymmetry. On the contrary, if the fissioning system emits many particles in the ground state region, then it will lose a greater part of the excitation energy. After passing through the saddle point this system will descend to the scission surface slowly along the bottom of the liquid-drop fission valley with  $\alpha' = 0$  and will never achieve a large mass asymmetry. Thus the final mass asymmetry and the fission time depend on the dynamical evolution of the fissioning nucleus in the ground state region. The smaller the neutrons emitted from the compound nucleus in the ground state region, the larger the probability of small fission time and large final mass asymmetry for the compound nucleus will be. The ratio  $\langle n_{pre}^{g.s.} \rangle / \langle n_{pre} \rangle$  determines the accessible phase space for the trajectory during the descent from the relevant conditional saddle-point configurations to the scission surface. As can be seen from Table I, the coefficient  $c_{pre}$  increases with  $k_s$  due to increase in presaddle particle emission. The ratio  $\langle n_{pre}^{g.s.} \rangle / \langle n_{pre} \rangle$  increases, hence the accessible phase space decreases, during the descent from the relevant conditional saddle-point configurations to the scission surface.

In order to verify our hypothesis we carried out calculations for the compound nucleus  $^{215}\text{Fr}$  where evaporation was not allowed before the saddle point was reached. All precission particles were emitted only during the descent from the relevant conditional saddle-point configurations to scission surface ( $\langle n_{pre}^{g.s.} \rangle = 0$ ). This assumption means that all Langevin trajectories reach the relevant conditional saddle-point configurations with an approximately equal excitation energy and, as a result, they will have the approximately equal accessible phase space during the descent from the relevant conditional saddle-point configurations to the scission sur-

TABLE I. Calculated results for the fission of  $^{172}\text{Yb}$ ,  $^{205}\text{Fr}$ ,  $^{215}\text{Fr}$ ,  $^{252}\text{Fm}$ , and  $^{256}\text{Fm}$  formed in the reactions:  $^{18}\text{O}+^{154}\text{Sm}\rightarrow^{172}\text{Yb}$  ( $E_{\text{lab}}=159$  MeV);  $^{36}\text{Ar}+^{169}\text{Tm}\rightarrow^{205}\text{Fr}$  ( $E_{\text{lab}}=205$  MeV);  $^{18}\text{O}+^{197}\text{Au}\rightarrow^{215}\text{Fr}$  ( $E_{\text{lab}}=159$  MeV);  $^{20}\text{Ne}+^{232}\text{Th}\rightarrow^{252}\text{Fm}$  ( $E_{\text{lab}}=215$  MeV);  $^{18}\text{O}+^{238}\text{U}\rightarrow^{256}\text{Fm}$  ( $E_{\text{lab}}=159$  MeV). The columns contain (from left to right) the compound nucleus (CN), the excitation energy ( $E^*$ ), the reduction coefficient of surface-plus-window dissipation  $k_s$ , the variance of the mass and kinetic-energy distributions of fission fragments ( $\sigma_M^2$  and  $\sigma_{E_K}^2$ ), the average total kinetic energy ( $\langle E_K \rangle$ ), the ratio  $\langle n_{\text{pre}}^{\text{g.s.}} \rangle / \langle n_{\text{pre}} \rangle$  that indicates the ground-state-saddle contribution to the precission neutron multiplicity  $\langle n_{\text{pre}} \rangle$ , the ratio  $\langle t_f^{\text{asym}} \rangle / \langle t_f^{\text{sym}} \rangle$  (see explanation in text), the average time of collective motion of the compound nucleus from its formation to the scission configurations ( $\langle t_f \rangle$ ), and the mean precission neutron multiplicity ( $\langle n_{\text{pre}} \rangle$ ).

CN	$E^*$ (MeV)	$k_s$	$c_{\text{pre}}$ $10^{-4}$	$\sigma_M^2$ ( $u^2$ )	$\sigma_{E_K}^2$ ( $\text{MeV}^2$ )	$\langle E_K \rangle$ (MeV)	$\langle n_{\text{pre}}^{\text{g.s.}} \rangle / \langle n_{\text{pre}} \rangle$	$\langle t_f^{\text{asym}} \rangle / \langle t_f^{\text{sym}} \rangle$	$\langle t_f \rangle$ ( $10^{-21}$ s)	$\langle n_{\text{pre}} \rangle$
$^{172}\text{Yb}$	121	0.25	20	$250 \pm 23$	$141 \pm 13$	110	0.99	0.74	54	3.4
		0.5	32	$160 \pm 14$	$52 \pm 5$	112.5	0.99	0.86	95	4.5
Expt. [1]			$14 \pm 1$	228	112	113				4.4
$^{205}\text{Fr}$	77	0.25	1.	$258 \pm 11$	$126 \pm 5$	154	0.82	0.97	27	0.4
		0.5	1.5	$238 \pm 14$	$104 \pm 6$	152	0.85	0.89	65	0.9
Expt. [2]			$0 \pm 0.1$	350	193	$151 \pm 8$				1.2
$^{215}\text{Fr}$	111	0.25	5.1	$331 \pm 13$	$189 \pm 10$	159	0.88	0.71	37	3
		0.5	7.1	$276 \pm 6$	$113 \pm 6$	157.5	0.91	0.62	89	4.3
Expt. [1]			$6.5 \pm 0.5$	272	190	154				4.1
$^{256}\text{Fm}$	101	0.25	1.6	$353 \pm 12$	$157 \pm 6$	201	0.66	0.96	15	2
		0.5	3.6	$283 \pm 10$	$139 \pm 5$	200	0.72	0.86	32	3.1
Expt. [1]			$8.2 \pm 1.2$	543	420	181				5.1
$^{252}\text{Fm}$	140	0.25	2.7	$393 \pm 11$	$219 \pm 7$	203	0.62	0.95	11	2.7
		0.5	3.6	$331 \pm 12$	$174 \pm 6$	202	0.7	0.9	22	4.0
Expt. [7]			0	643	411	195				6.95

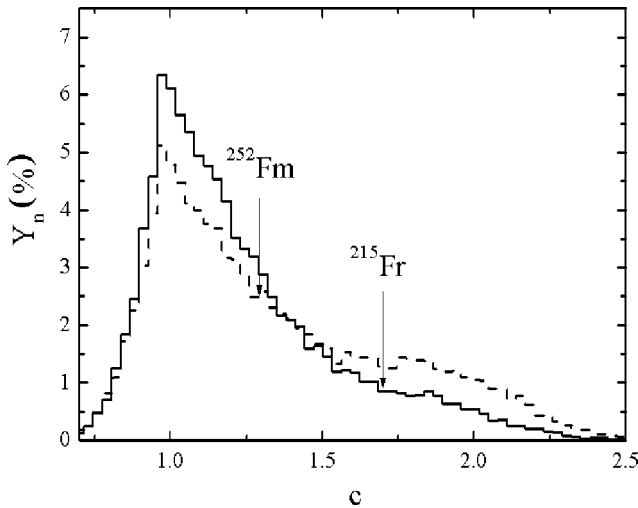


FIG. 2. The histograms are the percentage yield of the precission neutrons calculated with the reduction coefficient  $k_s=0.5$  (solid histogram) for the compound nucleus  $^{215}\text{Fr}$ , and  $k_s=0.25$  (dashed histogram) for the compound nucleus  $^{252}\text{Fm}$  as a function of the elongation parameter  $c$ . The arrows indicate the location of the saddle points.

face. In this case, as can be seen in Fig. 1,  $\langle t_f(M) \rangle$  and  $\langle n_{\text{pre}}(M) \rangle$  are nearly independent of  $M$  ( $c_{\text{pre}}=1.2 \times 10^{-4}$ ).

The calculated dependences  $\langle t_f(M) \rangle$  and  $\langle n_{\text{pre}}(M) \rangle$  are independent within statistical error range of the fragment mass asymmetry for the compound nuclei  $^{252}\text{Fm}$  at excitation energy  $E^*=140$  MeV and  $^{256}\text{Fm}$  at  $E^*=101$  MeV. The calculated values of  $c_{\text{pre}}$  are presented in Table I. The evaporation of light precission particles cannot reduce the accessible phase space considerably for these compound nuclei due to high excitation energy and small fission time and, as a result,  $\langle t_f(M) \rangle$  and  $\langle n_{\text{pre}}(M) \rangle$  are nearly independent of  $M$ .

The fission fragment mass distributions and dependences  $\langle n_{\text{pre}}(M) \rangle$  for the compound nucleus  $^{205}\text{Fr}$  are presented in Fig. 3. The experimental data and our calculations show that  $\langle n_{\text{pre}}(M) \rangle$  is independent of  $M$  for the compound nucleus  $^{205}\text{Fr}$ . At the same time, the excitation energy for the compound nucleus  $^{205}\text{Fr}$  is less than that for the compound nucleus  $^{215}\text{Fr}$ . The ratio  $\langle n_{\text{pre}}^{\text{g.s.}} \rangle / \langle n_{\text{pre}} \rangle$  for the compound nucleus  $^{205}\text{Fr}$  is equal to 0.9 and one can expect the parabolic mass dependence of  $\langle n_{\text{pre}}(M) \rangle$  and  $\langle t_f(M) \rangle$ . However, the compound nucleus  $^{205}\text{Fr}$  is very neutron deficient and all fissioning systems will have the approximately equal excitation energy due to the fact that the mean precission neutron multiplicity does not exceed one and evaporation of light-

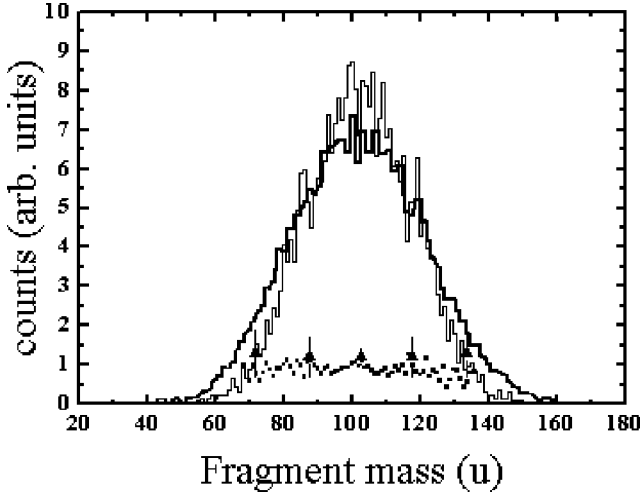


FIG. 3. The mass distribution (thick solid histogram) measured in coincidence with the precession neutron multiplicities  $\langle n_{\text{pre}}(M) \rangle$  (filled circles) is compared with the theoretical calculations for the compound nucleus  $^{205}\text{Fr}$ . The experimental data have been taken from Ref. [2]. The thin solid histogram and filled squares correspond to the mass distribution and the precession neutron multiplicities calculated with  $k_s = 0.5$ .

precession particles is only one way to reduce the total excitation energy. As a result, all fissioning systems will have the approximately equal accessible phase space during the descent from the relevant conditional saddle-point configurations to the scission surface.

The dependence  $\langle n_{\text{pre}}(M) \rangle$  was investigated earlier by Dhara and co-workers [9] in the two-dimensional model based on the Euler-Lagrange equations using a combination of both one-body and two-body nuclear dissipations. In Ref. [9] the components of the friction tensor were multiplied by  $\exp(-K\alpha^2)$ , where  $K = 161 \pm 3$ . Such a considerable reduction of dissipation leads to a decrease of the fission time for large mass asymmetries and, as a result, makes it possible to reproduce in calculations the parabolic dependence  $\langle n_{\text{pre}}(M) \rangle$ . Reproduction of the experimental dependence  $\langle n_{\text{pre}}(M) \rangle$  was impossible without inclusion of the factor  $\exp(-K\alpha^2)$  into the expression for the friction tensor in calculations [9].

Rossner and co-workers [2] found an unexpected increase of  $\langle n_{\text{pre}} \rangle$  with  $E_K$ . However, it turned out soon [3] that the deduced unexpected dependence  $\langle n_{\text{pre}}(E_K) \rangle$  was an artifact due to the recoil effect imparted by the emitted neutrons to the fission fragments. After the correction of this effect it was found [1,3] that  $\langle n_{\text{pre}}(E_K) \rangle$  was independent of  $E_K$ . In our calculations the mean fission time  $\langle t_f(E_K) \rangle$  and, as a result,  $\langle n_{\text{pre}}(E_K) \rangle$ , are nearly independent of  $E_K$  and slightly decrease only in the region of small  $E_K$  (see Fig. 4) for all compound nuclei considered in this paper. Such behavior of  $\langle n_{\text{pre}}(E_K) \rangle$  can be explained by using the dependence of the potential energy on the collective coordinates  $h, \alpha'$ . The potential energy surface is displayed in Figs. 5 and 6. As can be seen from these figures the potential energy depends on  $h$  more weakly than on  $\alpha'$ . Moreover, the stiffness with respect to the mass asymmetry coordinate  $\alpha'$  increases during the

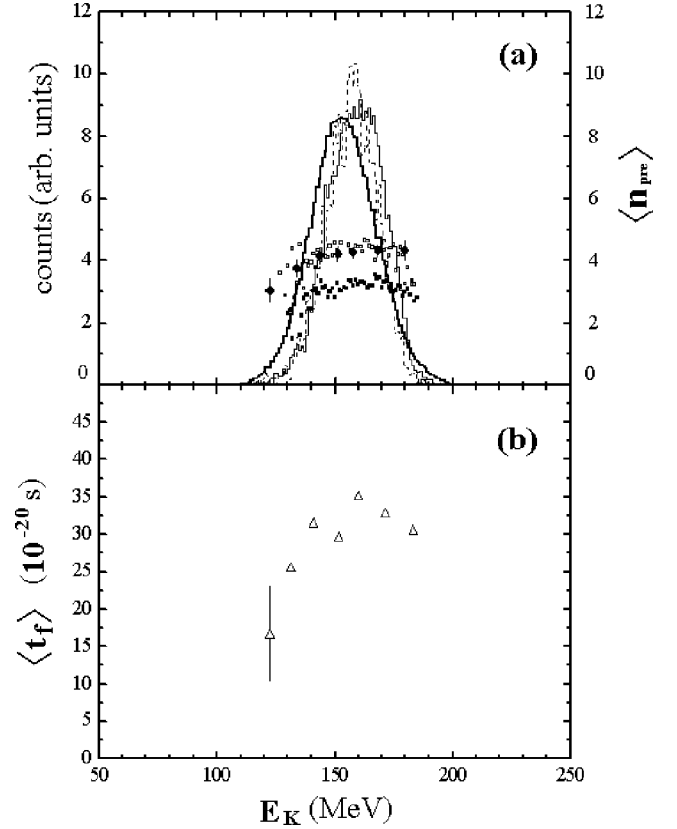


FIG. 4. (a) The kinetic-energy distribution (thick solid histogram) measured in coincidence with the precession neutron multiplicities  $\langle n_{\text{pre}}(E_K) \rangle$  (filled circles) is compared with the theoretical calculations for the compound nucleus  $^{215}\text{Fr}$ . The experimental data have been taken from Ref. [1]. The thin solid histogram and filled squares correspond to the energy distribution and the precession neutron multiplicities calculated with  $k_s = 0.25$ , whereas the dashed histogram and open squares correspond to the results with  $k_s = 0.5$ . (b) The open triangles are the theoretical energy dependence of the fission time calculated with  $k_s = 0.5$ .

descent from the saddle point to the scission surface, whereas the stiffness with respect to the constriction coordinate  $h$  decreases. The accessible phase space steadily decreases with respect to mass asymmetry coordinate  $\alpha'$  and remains approximately fixed with respect to the constriction parameter  $h$  during the descent from the relevant conditional saddle-point configurations to the scission surface. Trajectories even with small excitation energies have the opportunity to walk in a wide interval of  $h$ . The value of  $h$  at the scission surface determines the value of  $E_K$ . Thus, the value of  $E_K$  is nearly independent of the compound nucleus excitation energy in the region of the relevant conditional saddle-point configurations. In other words, the value of  $E_K$  is independent of the ratio  $\langle n_{\text{pre}}^{g.s.} \rangle / \langle n_{\text{pre}} \rangle$ . The decrease of the  $\langle n_{\text{pre}}(E_K) \rangle$  in the region of small  $E_K$  is related to the increase of contribution of the trajectories with large final mass asymmetries and small values of  $\langle n_{\text{pre}} \rangle$  [see Fig. 1(a)]. It should be stressed that the three-dimensional Langevin calculations with the modified one-body dissipation mechanism reproduce the dependence of  $\langle n_{\text{pre}}(E_K) \rangle$  better than the two-dimensional Langevin calculations [8] with the two-body nuclear dissipation.

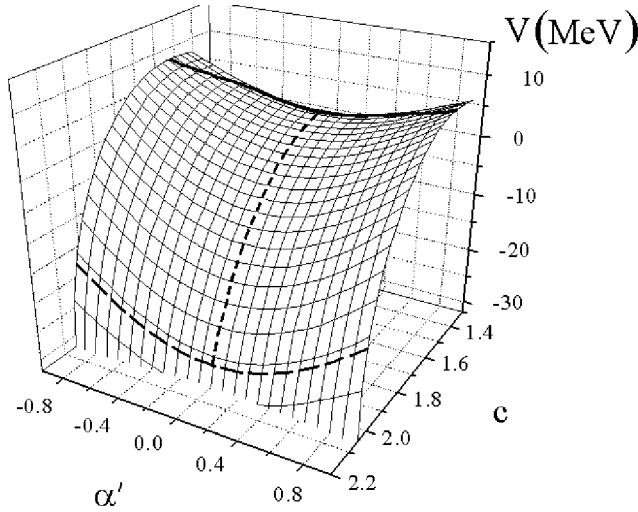


FIG. 5. The potential energy surface for the compound nucleus  $^{252}\text{Fm}$  in the case of  $h=0$  at zero angular momentum. The thick solid curve corresponds to the conditional saddle-point configurations. The short dashed curve is the mean dynamical trajectory. The dashed curve corresponds to the scission configurations and determined from the intersection of the scission surface and the plane  $h=0$ .

### B. Influence of the precession neutron evaporation on the anisotropy of the fission fragment angular distribution

In this and next subsections the following observables will be considered from the point of view of information on the fission dynamics (in particular on nuclear dissipation): the angular distributions in correlation with the precession neutron multiplicities, the evaporation residue cross sections, the fission probabilities, the parameters of the fission fragment MED, and the giant dipole  $\gamma$  multiplicities. The calcu-

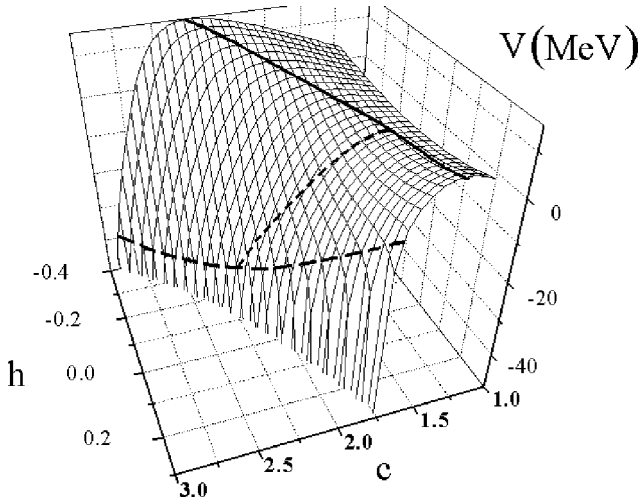


FIG. 6. The potential energy surface for the compound nucleus  $^{252}\text{Fm}$  in the case of  $\alpha'=0$  at zero angular momentum. The thick solid curve corresponds to the conditional saddle-point configurations. The short dashed curve is the mean dynamical trajectory. The dashed curve corresponds to the scission configurations and determined from the intersection of the scission surface and the plane  $\alpha'=0$ .

lations have been performed for the  $^{16}\text{O}+^{208}\text{Pb}$ -induced fission of  $^{224}\text{Th}$ . It should be mentioned that in Refs. [20,41] the one-dimensional Langevin models have been applied for the first time to study the main features of the angular distributions.

In the present paper the standard transition state model [42] has been used to analyze the fission fragment angular distributions. It is assumed that the equilibrium distribution on the  $K$  degree of freedom ( $K$  is the projection of the compound nucleus spin  $I$  onto the symmetry axis) is established at the transition state that is usually assumed to be the saddle point. In the case of the multidimensional model, a set of the relevant conditional saddle points play the role of the transition states. A frequently used approximation to the fission fragment angular distributions involves a computation of the following expression:

$$W(\theta, I) = \frac{(2I+1) \exp[-p \sin^2 \theta] J_0[-p \sin^2 \theta]}{\text{erf}[\sqrt{2p}]}, \quad (9)$$

where  $J_0$  is the zeroth-order Bessel function,  $p = (I + 1/2)^2 / (4K_0^2)$ , and the variance of the equilibrium  $K$ -distribution  $K_0$  is

$$K_0^2 = \frac{J_{\text{eff}}}{\hbar^2} T_{\text{sd}}, \quad J_{\text{eff}}^{-1} = J_{\parallel}^{-1} - J_{\perp}^{-1}. \quad (10)$$

Here  $T_{\text{sd}}$ ,  $J_{\parallel}$ , and  $J_{\perp}$  are the nuclear temperature and the moments of inertia for rotations around the symmetry axis and a perpendicular axis taken at the transition state, respectively. Diffuseness of the nuclear surface is taken into account to calculate  $J_{\parallel}$  and  $J_{\perp}$ .

An average angular distribution is obtained by averaging the expression (9) over the stochastic trajectory ensemble at the transition states. Thus, the anisotropy of the fragment angular distribution is given by

$$A = \frac{\langle W(0^0) \rangle}{\langle W(90^0) \rangle}. \quad (11)$$

There are three factors that control the angular distribution: the initial spin distribution, the effective inertia moments, and the nuclear temperatures at the transition states. The problem of the initial momentum distribution has been widely discussed in literature often in connection with the angular distribution and it continues to be one of the obscure problems of the contemporary nuclear physics. The partial fusion cross sections are often parametrized as

$$\frac{d\sigma_{\text{fus}}(I)}{dI} = \frac{2\pi}{k^2} \frac{2I+1}{1 + \exp[(I-I_c)/\delta I]}, \quad (12)$$

where the explicit expressions for the parameters  $I_c$  and  $\delta I$  are taken from Ref. [23].

The set of all available transition states is defined by the potential energy landscape and, hence, by the number of the considered collective coordinates. At the same time, a particular ensemble of transition points appreciably depends on

the dynamics of the fission process and it is sensitive to practically all underlain model ingredients: the conservative force, the viscosity mechanism, the method to calculate the inertia coefficient, etc. It should be stressed that in the one-dimensional models there is the only transition state for each angular momentum in contrast to the multidimensional ones where the ensemble of the transition points exists. It can significantly shift the values of the angular anisotropies calculated in different models.

The last factor—the nuclear temperature in the relevant conditional saddle point is tightly bound with the mean precission neutron multiplicities and, consequently, with nuclear dissipation. Note, the transition state temperature is determined by the presaddle neutron multiplicity  $\langle n_{\text{pre}}^{\text{g.s.}} \rangle$ . The mean precission neutron multiplicity is governed by the average value of nuclear dissipation, while the ratio  $\langle n_{\text{pre}}^{\text{g.s.}} \rangle / \langle n_{\text{pre}} \rangle$  appreciably depends on the coordinate behavior of the friction tensor components. Moreover, we expect from the results obtained in Ref. [20] within the one-dimensional Langevin model that an influence of the particle evaporation on the angular distribution will be significant. Therefore, the study of the angular distributions together with the precission neutron multiplicities could be one of the sensitive probes not only to the magnitude but also to the mechanism of nuclear viscosity.

Influence of the precission particles' emission on the anisotropy of the angular distribution could be analyzed by varying the strength of nuclear dissipation. The calculations carried out with  $k_s = 0.25, 0.5$ , and  $1$  will be discussed and confronted below. Variation of the friction strength alters not only a number of emitted particles but also the dynamics of the fission process. We performed calculations with and without precission particle evaporation in order to investigate an influence of the particle emission on the fragment angular distribution purely. The values of angular anisotropy shown in Fig. 7(a) demonstrate a trivial result: the calculations carried out without particle emission give smaller values of the angular anisotropy than it has been obtained with evaporation of light particles. The purpose of this analysis is to study the magnitude of the particle evaporation effect. As it is seen, the effect is visible but not so large as it was expected from the results of Ref. [20].

It is seen from Fig. 8(a) that a good quantitative agreement with the experimental data on  $\langle n_{\text{pre}} \rangle$  is obtained for  $k_s = 0.5$  and  $1$ . Calculations with  $k_s = 0.25$  underestimate  $\langle n_{\text{pre}} \rangle$  at the entire energy interval. It is noteworthy that in Ref. [43] the precission neutron multiplicity has been investigated for the reaction  $^{40}\text{Ar} + ^{180}\text{Hf} \rightarrow ^{220}\text{Th}$  for the various energies ranging from  $E_{\text{lab}} = 180$  to  $249$  MeV. The averaged slope of the calculated precission neutron multiplicity as a function of  $E_{\text{lab}}$  is  $(dn_{\text{pre}}/dE_{\text{lab}})^{-1} = 27.1$  MeV/neutron. Our calculations give the values of the slope  $(dn_{\text{pre}}/dE_{\text{lab}})^{-1} = 38.0, 28.0$ , and  $21.8$  MeV/neutron for  $k_s = 0.25, 0.5$ , and  $1$ , respectively. It is seen that the calculated slope with  $k_s = 0.5$  is closer to the one from Ref. [43]. The calculated results on  $\langle n_{\text{pre}} \rangle$  for the other reactions studied in the paper are listed in Table I. One can see a good quantitative agreement with the experimental data obtained at  $k_s = 0.5$  for the compound nuclei  $^{179}\text{Yb}$  and  $^{205,215}\text{Fr}$ . At the

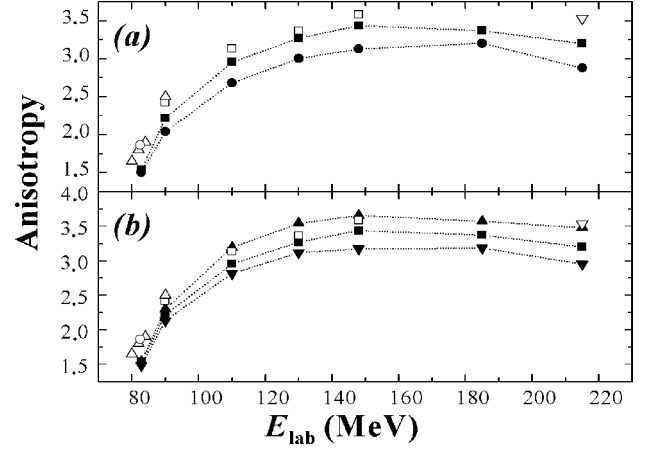


FIG. 7. The anisotropy of the fission fragment angular distribution as a function of the projectile laboratory energy for the reaction  $^{16}\text{O} + ^{208}\text{Pb} \rightarrow ^{224}\text{Th}$ : (a) the calculations with (filled squares) and without (filled circles) particle evaporation, respectively ( $k_s = 0.5$ ); (b) the calculations carried out for different values of the reduction coefficient:  $k_s = 0.25$  (inverted filled triangles),  $k_s = 0.5$  (filled squares), and  $k_s = 1$  (filled triangles). The calculated points are connected by dotted lines to guide the eye. The open symbols are the experimental data: Ref. [10] (circle), Ref. [11] (triangles), Ref. [15] (squares), and Ref. [16] (inverted triangle).

same time, for the heavier compound nuclei  $^{252,256}\text{Fm}$  the calculated values of  $\langle n_{\text{pre}} \rangle$  are appreciably less than the experimental ones. For these reactions the data can be reproduced only with full one-body dissipation but it leads to a strongly overdamped motion and, hence, to underestimation of the parameters of the fission fragment MED and the evaporation residue cross sections (see Secs. III C and III D for detailed discussion).

The energy dependences of the anisotropy of the angular distribution are shown in Fig. 7(b) for the same values of  $k_s$ . The behavior of the calculated values of the angular anisotropies and the experimental ones are in a qualitative agreement. Even at the high excitation energies our calculations reproduce a slight decrease of the anisotropy of the fragment angular distribution observed experimentally. This decrease can be explained in the following way. There are two opposite tendencies. On the one hand, the transition state temperature  $T_{\text{sd}}$  grows with the excitation energy that makes the  $K$ -distribution broader. On the other hand, in the region of low and intermediate energies the fusion cross sections increase exponentially with the excitation energy and the rapid growth of  $\langle I^2 \rangle$  determines increase of the angular anisotropy. At the higher excitation energies increase in  $T_{\text{sd}}$  equilibrates increase in  $\langle I^2 \rangle$ , further increasing of the excitation energy leads to the domination of the temperature factor over the  $\langle I^2 \rangle$  factor and the angular anisotropy decreases.

As regards a quantitative description, a satisfactory reproduction of the experimental data has been obtained at the values of the reduction coefficient  $k_s = 0.5-1$  at the whole energy interval, i.e., for such values of  $k_s$  that lead to a satisfactory quantitative description of the experimental data on  $\langle n_{\text{pre}} \rangle$ . One can see that the results obtained with  $k_s = 0.25, 0.5$ , and  $1$  differ from each other insignificantly up to  $E_{\text{lab}}$

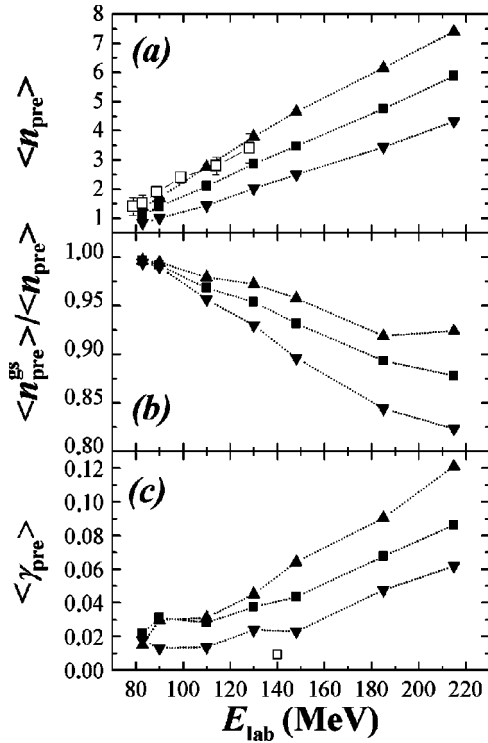


FIG. 8. The fission characteristics calculated as functions of the projectile laboratory energy for the reaction  $^{16}\text{O} + ^{208}\text{Pb} \rightarrow ^{224}\text{Th}$ . (a) the mean precission neutron multiplicity, the open symbols are the experimental data from Ref. [17]; (b) the ratio  $\langle n_{pre}^{g.s.} \rangle / \langle n_{pre} \rangle$ ; (c) the mean precission giant dipole  $\gamma$  multiplicity, the open symbol is the experimental datum from Ref. [22] (see the text for details). The calculated points are connected by dotted lines to guide the eye. The results calculated with different values of  $k_s$  are marked at the same order as in Fig. 7(b).

= 148 MeV. For the energies  $E_{lab} \geq 148$  MeV ( $E^* \geq 91$  MeV) the effect of  $k_s$  influence is the most significant and it is clearly seen that the calculations carried out with  $k_s = 0.25$  underestimates the experimental values of the angular anisotropy.

Thus, the following conclusions could be drawn after the calculated results for the angular anisotropies in correlation with the mean precission neutron multiplicities have been discussed. The proposed dynamical model leads to a good quantitative agreement with the experimental angular anisotropies and  $\langle n_{pre} \rangle$ . The anisotropy of the fragment angular distribution, contrary to our expectations, is less sensitive to the magnitudes of nuclear viscosity than the mean precission neutron multiplicities. The calculated angular anisotropies depend on  $k_s$  appreciably at high excitation energies only due to the most significant differences of  $\langle n_{pre} \rangle$ . Nevertheless, basing on the obtained results we conclude that an agreement with the experimental data on the mean neutron multiplicities is the necessary condition of the satisfactory quantitative description of the angular anisotropies.

Figure 8(b) shows the calculated results of the ratio  $\langle n_{pre}^{g.s.} \rangle / \langle n_{pre} \rangle$  for the different values of  $k_s$ . It is seen that the number of the saddle-scission neutrons increases with the excitation energy and decreases with increasing  $k_s$ . Note,

that the energy dependence of  $\langle n_{pre}^{g.s.} \rangle / \langle n_{pre} \rangle$  agrees qualitatively with that of Ref. [20], where the same reaction has been treated. The results obtained in Ref. [20] have allowed the authors to assert that agreement with the experimental data on the angular distribution for highly excited nuclei is possible only if a considerable part of precission neutrons is emitted on the descent of the fissioning nucleus from the saddle to scission. This part is about 3–5 times larger than it is predicted by our model for the same excitation energies, but we have obtained a good description of the data, too. It can be explained by the differences in the models. In our opinion the main difference is in the number of collective coordinates.

### C. The precission giant dipole $\gamma$ multiplicities, fission probabilities, and evaporation residue cross sections

As mentioned in Ref. [22] the mean precission giant dipole  $\gamma$  multiplicities and the evaporation residue cross sections (fission probabilities) are the most sensitive probes for nuclear dissipation in fission. The energy dependences of  $\langle \gamma_{pre} \rangle$  are shown in Fig. 8(c) for the three values of  $k_s$ . The experimental value at  $E_{lab} = 140$  MeV was taken from Ref. [22], where authors refer to private communications. We would like to remark that the precission  $\gamma$  multiplicities are sensitive to the viscosity magnitudes in the high-energy region. The value of  $\langle \gamma_{pre} \rangle$  calculated with  $k_s = 1$  at  $E_{lab} = 215$  MeV is about two times larger than one calculated with  $k_s = 0.25$ .

Figures 9(a) and 9(b) show the calculated energy dependences of  $P_f$  and  $\sigma_{ER}$  in comparison with the experimental data. The experimental values of the fission probabilities have been obtained by the relation  $P_f = \sigma_{fis} / (\sigma_{fis} + \sigma_{ER})$ , where the data on  $\sigma_{ER}$  are taken from Refs. [10,12] and the data on  $\sigma_{fis}$  from Refs. [10,14,15]. Some values of  $P_f$  have been estimated for  $\sigma_{ER}$  and  $\sigma_{fis}$  measured at unequal projectile energies due to the experimental data taken from the different works. The difference is 3.6 MeV for the point at  $E_{lab} = 133.6$  MeV and it does not exceed 1 MeV for the other points. It is seen from Figs. 9(a) and 9(b) that the fission probabilities and evaporation residue cross sections are in fact strongly influenced by the magnitudes of nuclear dissipation especially at low energies. The analysis of the excitation functions of  $P_f$  and  $\sigma_{ER}$  gives us a possibility to claim that the full one-body dissipation ( $k_s = 1$ ) can be rejected because a strong overestimation of  $\sigma_{ER}$  has been obtained. The experimental values lay between the curves calculated with  $k_s = 0.25$  and 0.5.

It has been mentioned above that in the present paper in contrast to our previous work [5] the free energy has been used as a driving potential instead of the bare potential energy. The calculations have shown that it has an appreciable effect on the evaporation residue cross sections. The energy dependences of  $\sigma_{ER}$  calculated for both types of the driving potential for  $k_s = 0.5$  are plotted in Fig. 9(c). It is seen that incorporation into the model of the free energy is a necessary step to a simultaneous description of the experimental data on  $\langle n_{pre} \rangle$ , on the anisotropy of the fragment angular distributions, and on the evaporation residue cross sections. Such a

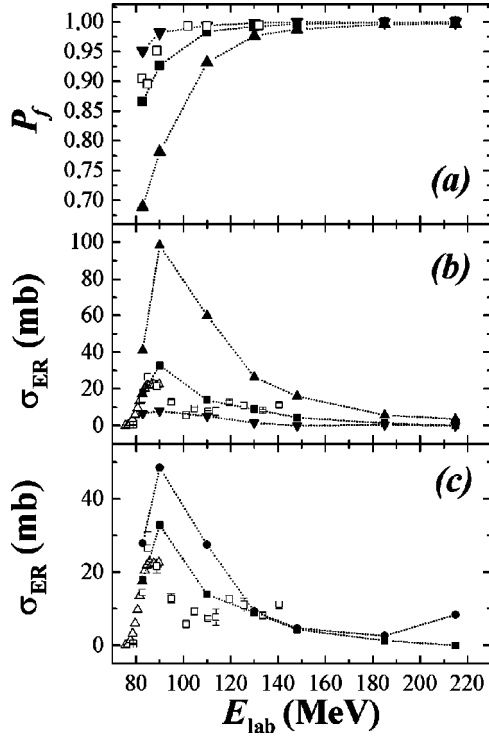


FIG. 9. The fission characteristics calculated as functions of the projectile laboratory energy for the reaction  $^{16}\text{O} + ^{208}\text{Pb} \rightarrow ^{224}\text{Th}$ . (a) The fission probability, open symbols are the experimental data (see the text for details); (b) the evaporation residue cross section, the open symbols are the experimental data from Ref. [10] (triangles), Ref. [12] (squares). The theoretical results calculated for different values of  $k_s$  are marked at the same order as in Fig. 7(b). (c) the evaporation residue cross section calculated with different types of the driving potential for  $k_s = 0.5$ : filled squares, the driving potential is the free energy, filled circles, the driving potential is the potential energy. The calculated points are connected by dotted lines to guide the eye.

simultaneous description could be obtained within the modified one-body dissipation model with the reduction coefficient  $k_s = 0.5$ , but not with the full one-body viscosity.

#### D. The parameters of the fission fragment MED and the mean precission neutron multiplicity

Finally, we would like to discuss our results concerning the mean precission neutron multiplicities and the parameters of the fission fragment MED. These observables have been analyzed carefully in our previous paper [5] and here we want to discuss only some additional aspects that influence the parameters of the fission fragment MED. Our calculated results and the experimental data from Refs. [1,2,7] are summarized in Table I and Figs. 8, 10. The calculated mass and energy distributions of fission fragments for the compound nuclei  $^{215}\text{Fr}$  and  $^{205}\text{Fr}$  are shown in Figs. 1(a), 3, and 4(a). For comparison, these figures also show the experimental distributions taken from Refs. [1,2]. As can be seen in Figs. 1(a), 3, and 4(a), the experimental mass and energy distributions are sufficiently well reproduced in the three-dimensional Langevin calculations. Both the experimental

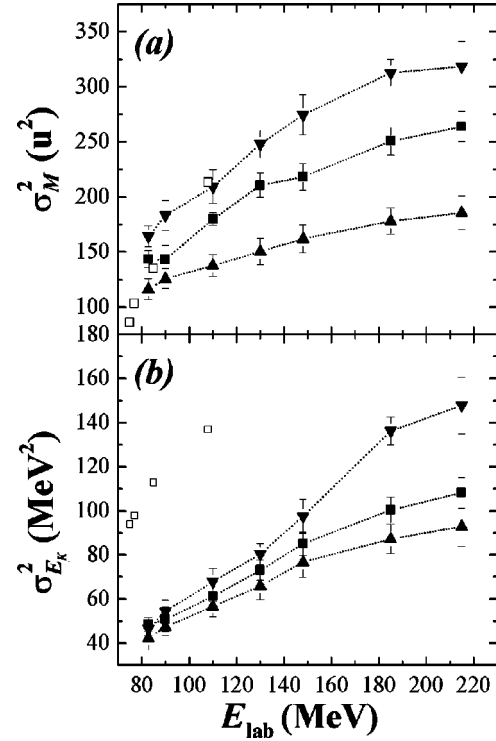


FIG. 10. The variance of the mass (a) and the kinetic-energy (b) distributions of the fission fragment MED as functions of the projectile laboratory energy for the reaction  $^{16}\text{O} + ^{208}\text{Pb} \rightarrow ^{224}\text{Th}$ . The open symbols are the experimental data [18]. The calculated points are connected by dotted lines to guide the eye. The results obtained with different values of  $k_s$  are marked at the same order as in Fig. 7(b).

and calculated mass distributions have a Gaussian-like form and can be characterized by the mean value  $\langle M \rangle$  and the variance  $\sigma_M^2$ . The calculated mass distribution becomes narrower when viscosity increases. This effect has been explained in detail early in Ref. [5].

The calculated parameters of the fission fragment MED and the mean precission neutron multiplicities are found to be in a good quantitative agreement with the experimental data for light fissioning systems ( $^{179}\text{Yb}$ ,  $^{205}\text{Fr}$ , and  $^{215}\text{Fr}$ ) at the values of the reduction coefficient  $k_s = 0.25 - 0.5$ . This result is consistent with our previous conclusions [5,6] made for the  $^{206}\text{Po}$  compound nucleus. As was noted earlier [5], simultaneous description of the fission fragment MED and the mean precission neutron multiplicities is impossible for heavy fissioning systems  $^{256}\text{Fm}$  and  $^{252}\text{Fm}$  at high excitation energy and angular momentum using the coordinate-independent reduction coefficient  $k_s$ . A quantitative agreement of the calculated results with the experimental data on the variances of the fission fragment MED can be achieved at the value of the reduction coefficient  $k_s \approx 0.1$ , but a good description of the mean precission neutron multiplicities is possible only at highly overdamped collective motion ( $k_s = 1$ ). However, the widths of the mass and kinetic-energy distributions calculated with  $k_s = 1$  are close to the statistical model predictions [44], which considerably underestimate values of the variances of the mass and energy distributions

for the fissioning nuclei with  $A_{\text{CN}} > 210$ . The similar result was obtained in Ref. [45] for the compound nuclei with  $A_{\text{CN}} > 260$ . It was shown that in order to reproduce the measured prescission neutron multiplicities the reduction coefficient must be increased by a factor ranging from  $k_s = 4$  to  $k_s = 12$ . Moreover, the calculations [45] were performed taking into account the stage of compound nucleus formation in contrast to our present calculations.

The calculated kinetic-energy distributions of fission fragments shown in Fig. 4(a) noticeably differ from the Gaussian distribution. They are not symmetrical with respect to the mean value  $\langle E_K \rangle$  and have sharper peaks than the Gaussian function. However, the experimental energy distribution [1] and those calculated in the two-dimensional model [8] have a more Gaussian-like form. Inclusion of the third collective coordinate (the mass asymmetry coordinate) in the two-dimensional model leads to a change in the shape and an increase in the width of the energy distribution. The calculated mean values of  $\langle E_K \rangle$  are found to be in a good quantitative agreement with the experimental data. The difference between calculated and experimental values of  $\langle E_K \rangle$  does not exceed 5% for light compound nuclei ( $^{172}\text{Yb}$ ,  $^{205}\text{Fr}$ , and  $^{215}\text{Fr}$ ) and 10% for heavy fissioning systems ( $^{252}\text{Fm}$  and  $^{256}\text{Fm}$ ). However, the calculated values of variance of the energy distributions are underestimated significantly for the  $k_s = 0.5$ . The reproduction of  $\sigma_{E_K}^2$  could be achieved for compound nuclei  $^{172}\text{Yb}$ ,  $^{205}\text{Fr}$ ,  $^{215}\text{Fr}$ , and  $^{224}\text{Th}$  by reducing the strength of nuclear dissipation to the value of  $k_s = 0.1-0.25$ . However, parameters of the energy distributions are very sensitive to the scission condition. In fact, at the present time there is no unambiguous criterion of the scission condition and we recognize that this intricate problem of the fission physics needs further detailed investigation in the framework of the finite-range LDM [31,46]. A quantitative analysis concerning the influence of the scission condition on the parameters of the energy distribution will be given in the forthcoming paper.

Three-dimensional Langevin calculations were performed earlier for the reactions  $^{19}\text{F} + ^{181}\text{Ta} \rightarrow ^{200}\text{Pb}$  ( $E_{\text{lab}} = 135$  MeV),  $^{16}\text{O} + ^{184}\text{W} \rightarrow ^{200}\text{Pb}$  ( $E_{\text{lab}} = 288$  MeV) in Refs. [32,33]. The full one-body dissipation ( $k_s = 1$ ) has been used in these calculations. Nevertheless, the calculated variances of the mass and energy distributions have been found to be in a good quantitative agreement with the experimental data in contradiction with our results. However, the calculations [32,33] show dependence of the parameters of the energy distributions on the parametrization of the nuclear shape. The values of  $\langle E_K \rangle$  and  $\sigma_{E_K}$  are about 15% larger for the two-center parametrization by Maruhn and Greiner [47] and Sato *et al.* [48] with fixed neck parameter than for the Legendre-polynomial parametrization [49]. So we can not expect a quantitative agreement between the results of our present calculations and results of previous three-dimensional Langevin calculations [32,33] due to the different parametrization of the nuclear shape. Moreover, the Coulomb repulsion energy at scission  $V_c$  has been determined approximately in Refs. [32,33], whereas we have calculated  $V_c$  and the nuclear attractive energy  $V_n$  of the nascent frag-

ments exactly in the finite-range LDM performing numerical evaluation of the corresponding integrals [50] (the procedure of the calculating  $E_K$  is described in our previous paper [5]). Finally, it should be stressed that calculations [32,33] were performed only for three values of the spin  $I = 30, 50, 70 \hbar$ , while we have parametrized the compound nuclei spin distribution according to the scaled prescription [23,51], which reproduces to a certain extent the dynamical results of the surface friction model [52] for fusion of two heavy ions.

#### IV. CONCLUSIONS

The three-dimensional stochastic approach to fission dynamics that has been successfully applied [5,6] for studying of the parameters of the fission fragment MED and the mean prescission neutron multiplicity is developed and extended to the calculation of the mass and kinetic-energy dependences of the prescission neutron multiplicities and excitation functions of some observable characteristics in fission in a broad range of the excitation energy. The conservative driving force of the Langevin equation and the statistical model expression for the fission width are governed by the free energy, not by the bare potential energy as in the previous calculations [5,6]. The functional of the free energy is constructed from the finite-range LDM as input for the potential energy and coordinate-dependent level density parameter that has been chosen according to Ignatyuk and collaborators [27].

The modified one-body mechanism of nuclear dissipation (so called surface-plus-window dissipation) was used to determine the dissipative forces of the Langevin equations. Under the assumption of the surface-plus-window dissipation mechanism of nuclear viscosity, the only variable parameter is the reduction coefficient of the contribution from a wall formula  $k_s$ .

We have calculated the two-dimensional fission fragment MED and the mean prescission neutron multiplicities in three-dimensional Langevin dynamics. The calculated parameters of the fission fragment MED, the dependences  $\langle n_{\text{pre}}(E_K) \rangle$ , and  $\langle n_{\text{pre}}(M) \rangle$  have been found to be in a good quantitative agreement with the available experimental data at the value of the reduction coefficient of the contribution from the wall formula [39]  $k_s = 0.25-0.5$  for the light fissioning compound systems  $^{172}\text{Yb}$ ,  $^{205}\text{Fr}$ , and  $^{215}\text{Fr}$ . The results of our calculations show that an appreciable part of the prescission neutrons is evaporated before the saddle point is reached for all compound nuclei considered in this study. The dependences  $\langle t_f(M) \rangle$  and  $\langle n_{\text{pre}}(M) \rangle$  are determined by the accessible phase space during the descent from the relevant conditional saddle-point configurations to the scission surface. The accessible phase space depends on the total excitation energy, the ratio  $\langle n_{\text{pre}}^{\text{g.s.}} \rangle / \langle n_{\text{pre}} \rangle$ , and other factors that influence the excitation energy distribution of fissioning systems in the region of the relevant conditional saddle-point configurations.

Choosing as an example the  $^{16}\text{O} + ^{208}\text{Pb}$  induced fission of  $^{224}\text{Th}$ , we have investigated the excitation functions of the following observable quantities: the mean prescission neutron and  $\gamma$  multiplicities, evaporation and fission cross sec-

tions, and anisotropy of fission fragment angular distribution. It is clearly seen that through a good quantitative description of the mean pre-scission neutron multiplicities, the fission probabilities and anisotropies could be achieved at the values of  $k_s = 0.5-1$ . At the same time the values of  $k_s = 0.1-0.2$  are necessary to reproduce the variances of the fission fragment MED. The simultaneous reproduction of  $\langle n_{pre} \rangle$  and the parameters of the fission fragment MED becomes more unsatisfactory for heavy fissioning systems  $^{252}\text{Fm}$  and  $^{256}\text{Fm}$ . From the analysis of these results one can conclude that coordinate-independent reduction coefficient  $k_s$  is not compatible with the simultaneous description of the main fission characteristics for heavy compound nuclei  $^{252}\text{Fm}$  and  $^{256}\text{Fm}$  and reduction coefficient  $k_s$  might depend not only on the fissility parameter as was noted in our previous calculations [5,6], but also on the collective coordinate and excitation energy. Such a kind of analysis has been extensively implemented in Refs. [20,21,23,28].

Last but not least, there is a hope that the microscopic approach based on the linear response theory [53–55] will shed light upon the problem of nuclear dissipation in fission and its coordinate and temperature dependence. Some results of the investigations in this direction have been reported in Refs. [56,57]. Unfortunately, almost no direct comparison of microscopically derived dissipation in fission with experimental results has been done so far. Another microscopic

approach to modification of a wall formula was also suggested in Refs. [58–60] in which the value of the reduction coefficient  $k_s$  was determined by a measure of chaos in single-particle motion of the nucleons within the nuclear volume. A measure of chaos (chaosity) depends on the instantaneous shape of the nucleus i.e., on the collective coordinates. The value of chaosity changes in the limits from 0 to 1 as the nucleus evolves from a spherical shape to highly deformed one. The first application of this approach for calculation of fission widths of excited nuclei was published recently [61]. It is, therefore, extremely interesting to derive the coordinate and/or temperature dependences of the reduction coefficient from the above-mentioned microscopic approaches and to use them in analysis as presented in our study.

#### ACKNOWLEDGMENTS

We would like to thank Dr. A. Ya. Rusanov, Dr. D. V. Vanin, and Dr. V. A. Drozdov for numerous enlightening discussions and correspondence. We are grateful to Dr. P. Fröbrich for support of this study and for constructive suggestions and critical comments that largely determined the contents of the present paper. We are indebted to Dr. O. V. Lakhina for a careful reading of the manuscript.

- 
- [1] D. J. Hinde, D. Hilscher, H. Rossner, B. Gebauer, M. Lehmann, and M. Wilpert, *Phys. Rev. C* **45**, 1229 (1992); D. J. Hinde, D. Hilscher, and H. Rossner, *Nucl. Phys. A* **538**, 243c (1992).
- [2] H. Rossner, D. Hilscher, D. J. Hinde, B. Gebauer, M. Lehmann, M. Wilpert, and E. Mordhorst, *Phys. Rev. C* **40**, 2629 (1989).
- [3] H. Rossner, D. Hilscher, and D. J. Hinde, *Phys. Rev. C* **43**, 2434 (1991).
- [4] D. Hilscher and H. Rossner, *Ann. Phys. (Paris)* **17**, 471 (1992).
- [5] A. V. Karpov, P. N. Nadtochy, D. V. Vanin, and G. D. Adeev, *Phys. Rev. C* **63**, 054610 (2001).
- [6] P. N. Nadtochy, A. V. Karpov, D. V. Vanin, and G. D. Adeev, *Yad. Fiz.* **64**, 926 (2001) [*Phys. At. Nucl.* **64**, 861 (2001)].
- [7] D. J. Hinde, H. Ogata, M. Tanaka, T. Shimoda, N. Takahashi, A. Shinohara, S. Wakamatsu, K. Katori, and H. Okamura, *Phys. Rev. C* **39**, 2268 (1989).
- [8] G.-R. Tillack, R. Reif, A. Schülke, P. Fröbrich, H. J. Krappe, and H. G. Reusch, *Phys. Lett. B* **296**, 296 (1992).
- [9] A. K. Dhara, K. Krishan, C. Bhattacharya, and S. Bhattacharya, *Phys. Rev. C* **57**, 2453 (1998); *Eur. Phys. J. A* **7**, 209 (2000).
- [10] C. R. Morton, D. J. Hinde, J. R. Leigh, J. P. Lestone, M. Dasgupta, J. C. Mein, J. O. Newton, and H. Timmers, *Phys. Rev. C* **52**, 243 (1995).
- [11] E. Vulgaris, L. Grodzins, S. G. Steadman, and R. Ledoux, *Phys. Rev. C* **33**, 2017 (1986).
- [12] K.-T. Brinkmann, A. L. Caraley, B. J. Fineman, N. Gan, J. Velkovska, and R. L. McGrath, *Phys. Rev. C* **50**, 309 (1994).
- [13] T. Murakami, C.-C. Sahm, R. Vandenbosch, D. D. Leach, A. Ray, and M. J. Murphy, *Phys. Rev. C* **34**, 1353 (1986).
- [14] F. Videbaek, R. B. Goldstein, L. Grodzins, and S. G. Steadman, *Phys. Rev. C* **3**, 954 (1977).
- [15] B. B. Back, R. R. Betts, J. E. Gindler, B. D. Wilkins, S. Saini, M. B. Tsang, C. K. Gelbke, W. G. Lynch, M. A. McMahan, and P. A. Baisden, *Phys. Rev. C* **32**, 195 (1985).
- [16] L. C. Vaz, D. Logan, E. Duek, J. M. Alexander, M. F. Rivet, M. S. Zisman, M. Kaplan, and J. W. Ball, *Z. Phys. A* **315**, 169 (1984).
- [17] H. Rossner, D. J. Hinde, J. R. Leigh, J. P. Lestone, J. O. Newton, J. X. Wei, and S. Elfström, *Phys. Rev. C* **45**, 719 (1992).
- [18] M. G. Itkis, Yu. Ts. Oganessian, G. G. Chubarian, V. S. Salamatin, A. Ya. Rusanov, and V. N. Okolovich, in *Proceedings of the XV EPS Conference on Low Energy Nuclear Dynamics (LEND-95), St. Petersburg, 1995*, edited by Yu. Ts. Oganessian, R. Kalpakchieva, and W. von Oertzen (World Scientific, Singapore, 1995), p. 177.
- [19] S. Kailas, *Phys. Rep.* **284**, 381 (1997).
- [20] P. Fröbrich and H. Rossner, *Z. Phys. A* **349**, 99 (1994).
- [21] I. I. Gontchar, and L. A. Litnevsky, *Z. Phys. A* **359**, 149 (1997).
- [22] P. Fröbrich and I. I. Gontchar, *Nucl. Phys. A* **563**, 326 (1993).
- [23] P. Fröbrich and I. I. Gontchar, *Phys. Rep.* **292**, 131 (1998).
- [24] M. Brack, J. Damgaard, A. S. Jensen, H. C. Pauli, V. M. Strutinsky, and C. Y. Wong, *Rev. Mod. Phys.* **44**, 320 (1972).
- [25] R. Balian and C. Bloch, *Ann. Phys. (N.Y.)* **60**, 401 (1970).
- [26] S. Cohen and W. J. Swiatecki, *Ann. Phys. (N.Y.)* **22**, 406 (1963).
- [27] A. V. Ignatyuk, M. G. Itkis, V. N. Okolovich, G. N. Smirenkin,

- and A. S. Tishin, *Yad. Fiz* **21**, 1185 (1975) [*Sov. J. Nucl. Phys.* **21**, 612 (1975)].
- [28] P. Fröbrich, I. I. Gontchar, and N. D. Mavlitov, *Nucl. Phys.* **A556**, 281 (1993).
- [29] H. J. Krappe, in *Proceedings of the International Workshop on Dynamical Aspects of Nuclear Fission, Smolenice, Slovakia, 1991*, edited by J. Kristiak and B. I. Pustylnik (JINR, Dubna, 1992), p. 51.
- [30] M. Brack, C. Guet, and H. B. Håkansson, *Phys. Rep.* **123**, 275 (1985).
- [31] H. J. Krappe, J. R. Nix, and A. J. Sierk, *Phys. Rev. C* **20**, 992 (1979).
- [32] Y. Abe, S. Ayik, P-G. Reinhard, and E. Suraud, *Phys. Rep.* **275**, 49 (1996).
- [33] T. Wada, in *Proceedings of the 2nd Tours Symposium on Nuclear Physics, Tours, 1994*, edited by H. Utsunomiya, M. Ohta, J. Galin, and G. Munzenberg (World Scientific, Singapore, 1995), p. 470; Y. Abe, in *Proceedings of the 3rd IN2P3-RIKEN Symposium on Heavy Ion Collisions, Tokyo, 1994*, edited by T. Motobayashi, N. Frascaria, and M. Ishihara (World Scientific, Singapore, 1995), p. 123.
- [34] T. Wada, N. Carjan, and Y. Abe, *Nucl. Phys.* **A538**, 283c (1992); T. Wada, Y. Abe, and N. Carjan, *Phys. Rev. Lett.* **70**, 3538 (1993).
- [35] K. T. R. Davies, R. A. Managan, J. R. Nix, and A. J. Sierk, *Phys. Rev. C* **16**, 1890 (1977).
- [36] N. D. Mavlitov, P. Fröbrich, and I. I. Gontchar, *Z. Phys. A* **342**, 195 (1992).
- [37] H. A. Weidenmüller and Zhang Jing-Shang, *J. Stat. Phys.* **34**, 191 (1984); Zhang Jing-Shang and H. A. Weidenmüller, *Phys. Rev. C* **28**, 2190 (1983).
- [38] P. Fröbrich and G. R. Tillack, *Nucl. Phys.* **A540**, 353 (1992).
- [39] J. R. Nix and A. J. Sierk, in *Proceedings of the 6th Adriatic Conference on Nuclear Physics: Frontiers of Heavy Ion Physics, Dubrovnik, Yugoslavia, 1987*, edited by N. Cindro, R. Caplar, and W. Greiner (World Scientific, Singapore, 1990), p. 333.
- [40] J. R. Nix and A. J. Sierk, in *Proceedings of the International School-Seminar on Heavy Ion Physics, Dubna, USSR, 1986*, edited by M. I. Zarubina and E. V. Ivashkevich (JINR, Dubna, 1987), p. 453; J. R. Nix, *Nucl. Phys.* **A502**, 609c (1989).
- [41] V. A. Drozdov, D. O. Eremenko, S. Yu. Platonov, O. V. Fotina, and O. A. Yuminov, *Yad. Fiz.* **64**, 221 (2001) [*Phys. At. Nucl.* **64**, 179 (2001)].
- [42] R. Vandenbosch and J. R. Huizenga, *Nuclear Fission* (Academic, New York, 1973).
- [43] V. A. Rubchenya *et al.*, *Phys. Rev. C* **58**, 1587 (1998).
- [44] P. Fong, *Statistical Theory of Nuclear Fission* (Gordon and Breach, New York, 1969).
- [45] J. Wilczyński, K. Siwek-Wilczyńska, and H. W. Wilschut, *Phys. Rev. C* **54**, 325 (1996).
- [46] A. J. Sierk, *Phys. Rev. C* **33**, 2039 (1986).
- [47] J. Maruhn and W. Greiner, *Z. Phys.* **251**, 431 (1972).
- [48] K. Sato, A. Iwamoto, K. Harada, S. Yamaji, and S. Yoshidata, *Z. Phys. A* **288**, 383 (1978).
- [49] N. Carjan, A. J. Sierk, and J. R. Nix, *Nucl. Phys.* **A452**, 381 (1986).
- [50] K. T. R. Davies and J. R. Nix, *Phys. Rev. C* **14**, 1977 (1976).
- [51] I. I. Gontchar, L. A. Litnevsky, and P. Fröbrich, *Comput. Phys. Commun.* **107**, 223 (1997).
- [52] J. Marten and P. Fröbrich, *Nucl. Phys.* **A545**, 854 (1992).
- [53] H. Hofmann, *Phys. Rep.* **284**, 137 (1997).
- [54] H. Hofmann and F. A. Ivanyuk, *Phys. Rev. Lett.* **82**, 4603 (1999).
- [55] F. A. Ivanyuk and H. Hofmann, *Nucl. Phys.* **A657**, 19 (1999).
- [56] H. Hofmann, F. A. Ivanyuk, C. Rummel, and S. Yamaji, *Phys. Rev. C* **64**, 054316 (2001).
- [57] F. A. Ivanyuk, H. Hofmann, V. V. Pashkevich, and S. Yamaji, *Phys. Rev. C* **55**, 1730 (1997).
- [58] S. Pal and T. Mukhopadhyay, *Phys. Rev. C* **54**, 1333 (1996).
- [59] T. Mukhopadhyay and S. Pal, *Phys. Rev. C* **56**, 296 (1997).
- [60] S. Pal and T. Mukhopadhyay, *Phys. Rev. C* **57**, 210 (1998).
- [61] G. Chaudhuri and S. Pal, *Phys. Rev. C* **63**, 064603 (2001).